DOI: 10.1002/ejic.200601089

Redox-Induced μ-Acetato and μ-Oxo Core Interconversions in Dinuclear Manganese Tris(2-methylpyridyl)amine (tpa) Complexes: Isolation and Characterization of $[Mn_2^{III}(\mu\text{-}O)(\mu\text{-}O_2CCH_3)(tpa)_2]^{3+}$

Marie-Noëlle Collomb,*[a] Claire Mantel,[a,b] Sophie Romain,[a] Carole Duboc,[b] Jean-Claude Leprêtre,[a] Jacques Pécaut,[c] and Alain Deronzier[a]

Keywords: Manganese / Electrochemistry / N ligands / Bridging ligands

The electrochemical properties of the bis(μ-acetato) complex $[Mn_2^{II}(O_2CCH_3)_2(tpa)_2]^{2+}$ ($\mathbf{1}^{2+}$) [tpa = tris(2-methylpyridyl)-amine] in an organic medium (CH_3CN) have been studied. Two successive controlled potential oxidations of a solution of $\mathbf{1}^{2+}$ at 0.7 and 1.1 V vs. Ag/Ag^+ (10 mM) allow the selective and nearly quantitative formation of the mono-(μ-oxo) mono-(μ-acetato) complex $[Mn_2^{III}(O)(O_2CCH_3)(tpa)_2]^{3+}$ ($\mathbf{2}^{3+}$) and the bis(μ-oxo) complex $[Mn_2^{IV}(O)_2(tpa)_2]^{4+}$ ($\mathbf{3}^{4+}$), respectively. These results show that each substitution of an acetate group by an oxo group is caused by an overall two-electron oxidation of the corresponding dimanganese complex. The associated electrochemical back transformations were also investigated. Complex $\mathbf{2}^{3+}$, which possesses a rare mono-(μ-oxo) mono-(μ-acetato) motif, has been isolated and characterized by X-ray crystallography. This complex crystallizes in the monoclinic system, space group $P2_1/n$ with a = 11.9899(17), b = 35.050(5), c = 12.3952(18) Å, β = 101.218(6)°, Z = 4.

Introduction

Much effort has been directed towards the chemistry of binuclear manganese complexes with oxo- and/or acetato-bridged cores due to their relevance to biological systems such as the manganese catalases (Mn Cat) and the oxygen-evolving complex (OEC) of photosystem II (PSII).[1–3] The active centers are a di- (MnCat) or a tetranuclear (OEC) manganese complex where oxidation states II, III, and IV are implicated during the enzymatic catalytic cycles. The MnCat switches between the Mn_2^{II} and Mn_2^{III} forms during the catalysis, and only these two oxidation states are able to catalyze the disproportionation of H_2O_2 at extremely high rates.[1] Recent structural characterizations[4–7] of the oxidized Mn_2^{III} form reveal a Mn–Mn separation of 3.03 to 3.4 Å and that the two metal centers are triply bridged by a $\mu_{1,3}$-carboxylate group of a glutamate (or aspartate) residue and two oxygen atoms, possibly one oxo and one hydroxo. EXAFS studies suggest that the Mn–Mn separation is significantly longer in the reduced Mn_2^{II} form of the enzyme (3.4 to 3.7 Å), such that both bridging oxygen atoms come from water and/or hydroxide.[8]

In contrast, the exact structure of the active center in PSII, as well as the mechanism of water oxidation, remain elusive.[2,9–15] During the catalytic cycle it is known that the tetranuclear manganese cluster in PSII cycles through five increasingly oxidized states, denoted as S_0–S_4. The most oxidized state, S_4, is unstable and relaxes back to S_0 with the release of O_2. On the basis of XAS and EPR data, it is generally accepted that the oxidation states in S_1 and S_2 are $Mn_2^{III}Mn_2^{IV}$ and $Mn^{III}Mn_3^{IV}$, respectively.[2,16] XAS studies have also provided evidence for the existence of Mn–(μ-O)$_2$–Mn (Mn–Mn distance of 2.7 Å) and Mn–(μ-O)–Mn (Mn–Mn distance of 3.3 Å) moieties in the tetramer,[17,18] while the recent crystal structures of PSII[19–23] suggest that the four metallic ions of the OEC are organized in a "3 + 1" fashion.

The oxidation state changes in both MnCat and PSII enzymes are accompanied by structural changes involving the groups bridging the Mn atoms. For example, the significant structural changes that occur during the $S_0 \rightarrow S_1$ and $S_2 \rightarrow S_3$ transitions in PSII have been identified as a deprotonation of a μ-hydroxo bridge and the formation of a third Mn–(μ-O)$_2$–Mn unit, respectively.[2,14] In addition, as suggested recently, the combination of bidentate carboxylate ligands and mono- or di-oxo bridges could enhance the stability of the cation arrangement and facilitate rearrangement of the μ-oxo bridges during the S-state cycle.[23]

[a] Laboratoire d'Electrochimie Organique et de Photochimie Rédox, Université Joseph Fourier, CNRS UMR 5630, Institut de Chimie Moléculaire de Grenoble (ICMG), FR CNRS 2607, Grenoble 1,
B. P. 53, 38041 Grenoble Cedex 9, France
Fax: +33-4-76514267
E-mail: Marie-Noelle.Collomb@ujf-grenoble.fr
[b] The Grenoble High Magnetic Field Laboratory, CNRS UPR 5021,
B. P. 166, 38042 Grenoble Cedex 9, France
[c] DRFMC-Service de Chimie Inorganique et Biologique, Laboratoire Coordination et Chiralité, CEA-Grenoble,
38054 Grenoble Cedex, France

μ-Acetato/μ-hydroxo or μ-oxo bridging ligand changes in relation to Mn oxidation have been reported for synthetic binuclear Mn complexes with multidentate ancillary N and/or O ligands.[24–34] Electrochemistry is a convenient way to investigate these kinds of redox-induced structural changes, and we have previously demonstrated the efficiency of the electrochemically induced core interconversion in an organic medium (CH_3CN) for the tris(μ-acetato) complex $[Mn_2^{II}(O_2CCH_3)_3(bpea)_2]^+$ [bpea = *N*,*N*-bis(2-methylpyridyl)ethylamine].[28,29] The mono-(μ-oxo) $[Mn_2^{III}(O)(O_2CCH_3)_2(bpea)_2]^{2+}$ and bis(μ-oxo) $[Mn_2^{IV}(O)_2(O_2CCH_3)(bpea)_2]^{3+}$ complexes have been selectively and quantitatively generated by an exhaustive electrochemical oxidation of $[Mn_2^{II}(O_2CCH_3)_3(bpea)_2]^+$. In order to evaluate the influence of the structure of the complex on the efficiency of the electrochemical process, we report here a similar study conducted with the bis(μ-acetato) complex $[Mn_2^{II}(O_2CCH_3)_2(tpa)_2]^{2+}$ ($\mathbf{1}^{2+}$) [tpa = tris(2-methylpyridyl)amine]. This latter complex contains tetradentate amino ligands instead of tridentate ones and only two acetate bridging ligands instead of three. The electrochemical synthesis of the mono-(μ-oxo) mono-(μ-acetato) complex $[Mn_2^{III}(O)(O_2CCH_3)(tpa)_2]^{3+}$ ($\mathbf{2}^{3+}$) and the redox properties of the bis(μ-oxo) complex $[Mn_2^{III,IV}(O)_2(tpa)_2]^{3+}$ ($\mathbf{3}^{3+}$) are also reported. Complexes $\mathbf{1}(TCNQ)_2\cdot CH_3CN$, $\mathbf{3}(BPh_4)_2$, and $\mathbf{3}(S_2O_6)_{3/2}\cdot 7H_2O$[35–37] have been structurally and spectroscopically characterized previously, and the electrochemical properties of $\mathbf{3}^{3+}$ have been briefly studied in CH_3CN.[37,38] In contrast, complex $\mathbf{2}^{3+}$, which possesses a rare mono-(μ-oxo) mono-(μ-acetato) motif,[39–41] has not been isolated previously and we report here its characterization by X-ray crystallography.

Results

Synthesis and Crystal Structure of $[Mn_2^{III}(\mu\text{-}O)(\mu\text{-}O_2CCH_3)(tpa)_2](PF_6)_3$ $[\mathbf{2}(PF_6)_3]$

This complex was obtained by preparative electrolysis of a concentrated solution of $\mathbf{1}^{2+}$ in CH_3CN containing 0.1 M Bu_4NPF_6. Slow diffusion of diethyl ether into this solution leads to single crystals of $\mathbf{2}(PF_6)_3\cdot CH_3CN$ in good yield (see Experimental Section). The structure of this complex was determined by X-ray diffraction. Figure 1 shows the structure of the $[Mn_2^{III}(\mu\text{-}O)(\mu\text{-}O_2CCH_3)(tpa)_2]^{3+}$ cation and the atom labelling scheme; Table 1 summarises important bond lengths and angles. Each manganese atom exhibits a highly distorted octahedral geometry and is bound by four nitrogen atoms from a single tpa ligand and two oxygen atoms, one from the bridging oxo group and the other from the bridging acetate.

The $\{Mn_2(O)(O_2CCH_3)\}^{3+}$ core of the complex yields a Mn···Mn distance of 3.253(3) Å. To the best of our knowledge, only four other crystallographically characterized complexes possess this type of core. In $[Mn_2^{III}(O)(O_2CCH_3)(bispicen)_2]^{3+}$ [bispicen = *N*,*N*′-bis(2-methylpyridyl)ethane-1,2-diamine] and $[Mn_2^{III}(O)(O_2CCH_3)(bispicMe_2en)_2]^{3+}$ [bispicMe$_2$en = *N*,*N*′-dimethyl-*N*,*N*′-bis(2-methylpyridyl)ethane-1,2-diamine],[39] the Mn···Mn distances are 3.276(3) and 3.292(14) Å, respectively, whereas in $[Mn_2^{III}(O)(O_2CCH_3)(tmima)_2]^{2+}$ [tmima = tris(1-methylimidazol-2-yl)methylamine][40] and $[Mn_2^{III}(O)(O_2CCH_3)(bpia)_2]^{3+}$ [bpia = bis(picolyl)(*N*-methylimidazol-2-yl)amine][41] the two manganese ions are separated by 3.250(1) and 3.2544(8) Å, respectively. Compared to the other crystallographically characterized dimanganese tpa complexes, the Mn···Mn distance in $\mathbf{2}^{3+}$ is significantly longer than those found in the bis(μ-oxo) complexes at the (III,III) and (III,IV) oxidation level [2.656(2) Å ($\mathbf{3}^{2+}$)[36] and 2.643(1) Å ($\mathbf{3}^{3+}$)[37]] and shorter than that in the bis(μ-acetato) complex [4.154(1) Å ($\mathbf{1}^{2+}$)].[35] A noticeable compression of the bond

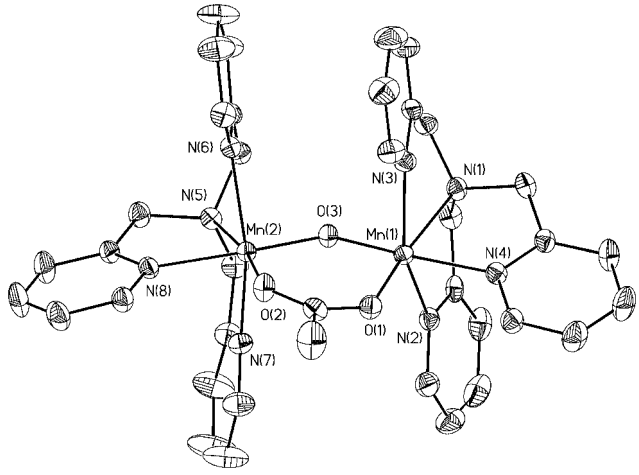

Figure 1. ORTEP view of the cation $[Mn_2^{III}(O)(O_2CCH_3)(tpa)_2]^{3+}$ ($\mathbf{2}^{3+}$).

Table 1. Selected bond lengths [Å] and angles [°] for $\mathbf{2}(PF_6)_3\cdot CH_3CN$.

Mn(1)–Mn(2)	3.253(3)		
Mn(1)–N(1)	2.187(3)	Mn(2)–N(5)	2.168(3)
Mn(1)–N(2)	2.163(3)	Mn(2)–N(6)	2.193(3)
Mn(1)–N(3)	2.194(3)	Mn(2)–N(7)	2.201(3)
Mn(1)–N(4)	2.048(3)	Mn(2)–N(8)	2.058(3)
Mn(1)–O(1)	1.987(2)	Mn(2)–O(2)	1.987(2)
Mn(1)–O(3)	1.778(2)	Mn(2)–O(3)	1.786(2)
Mn(1)–O(3)–Mn(2)	131.82(3)		
N(1)–Mn(1)–N(2)	78.68(11)	N(5)–Mn(2)–N(6)	75.85(11)
N(1)–Mn(1)–N(3)	75.38(11)	N(5)–Mn(2)–N(7)	78.27(11)
N(1)–Mn(1)–N(4)	80.80(11)	N(5)–Mn(2)–N(8)	80.82(11)
N(2)–Mn(1)–N(3)	154.00(11)	N(6)–Mn(2)–N(7)	153.91(11)
N(2)–Mn(1)–N(4)	83.87(11)	N(6)–Mn(2)–N(8)	89.71(11)
N(3)–Mn(1)–N(4)	90.22(12)	N(7)–Mn(2)–N(8)	82.93(12)
O(1)–Mn(1)–O(3)	98.29(11)	O(2)–Mn(2)–O(3)	98.49(11)
O(1)–Mn(1)–N(1)	166.49(12)	O(2)–Mn(2)–N(5)	170.68(12)
O(1)–Mn(1)–N(2)	109.05(11)	O(2)–Mn(2)–N(6)	105.87(11)
O(1)–Mn(1)–N(3)	96.08(11)	O(2)–Mn(2)–N(7)	99.15(11)
O(1)–Mn(1)–N(4)	88.90(11)	O(2)–Mn(2)–N(8)	89.99(11)
O(3)–Mn(1)–N(1)	92.45(11)	O(3)–Mn(2)–N(5)	90.65(11)
O(3)–Mn(1)–N(2)	91.42(11)	O(3)–Mn(2)–N(6)	89.72(11)
O(3)–Mn(1)–N(3)	91.45(11)	O(3)–Mn(2)–N(7)	93.85(11)
O(3)–Mn(1)–N(4)	172.40(11)	O(3)–Mn(2)–N(8)	171.32(11)

lengths along the $N_{pyridine}$(4 or 8)–Mn–O_{oxo}(3) axis is observed in $\mathbf{2}^{3+}$ due to the Jahn–Teller effect expected for a high-spin d^4 Mn^{III} ion. Although this kind of distortion is rarely observed for a Mn^{III} ion, a similar tetragonal compression occurs in the four other complexes with the same core.[39–41] The Mn–O_{oxo}–Mn angle of 131.82(3)° in $\mathbf{2}^{3+}$ is comparable to those found in the four other complexes (130.9° < Mn–O_{oxo}–Mn < 133°). The Mn–O_{oxo} bond lengths of 1.778(2) and 1.786(2) Å and the Mn–$O_{acetate}$ distance of 1.987(3) Å in $\mathbf{2}^{3+}$ are consistent with the corresponding bond lengths reported for the parent complexes [1.784(3) < Mn–O_{oxo} < 1.801(3) Å and 1.90(3) < Mn–O_{carb} < 2.042(4) Å].[39–41] The Mn–$N_{pyridine}$(4 and 8) bonds [2.048(3) and 2.058(3) Å] *trans* to the oxo group are considerably shorter than the other Mn–$N_{pyridine}$ bond lengths due to the compression of the octahedron [Mn(1)–N(2) 2.163(3), Mn(1)–N(3) 2.194(3), Mn(2)–N(6) 2.193(3), Mn(2)–N(7) 2.201(3) Å]. The distortions from octahedral geometry observed around the Mn ions are also due to the spatially constrained nature of the tetradentate tpa ligand, as revealed by the values of the N_{amine}–Mn–$N_{pyridine}$ intraligand angles, which range between 75.38° and 90.22° (Table 1); the theoretical value is 90°.

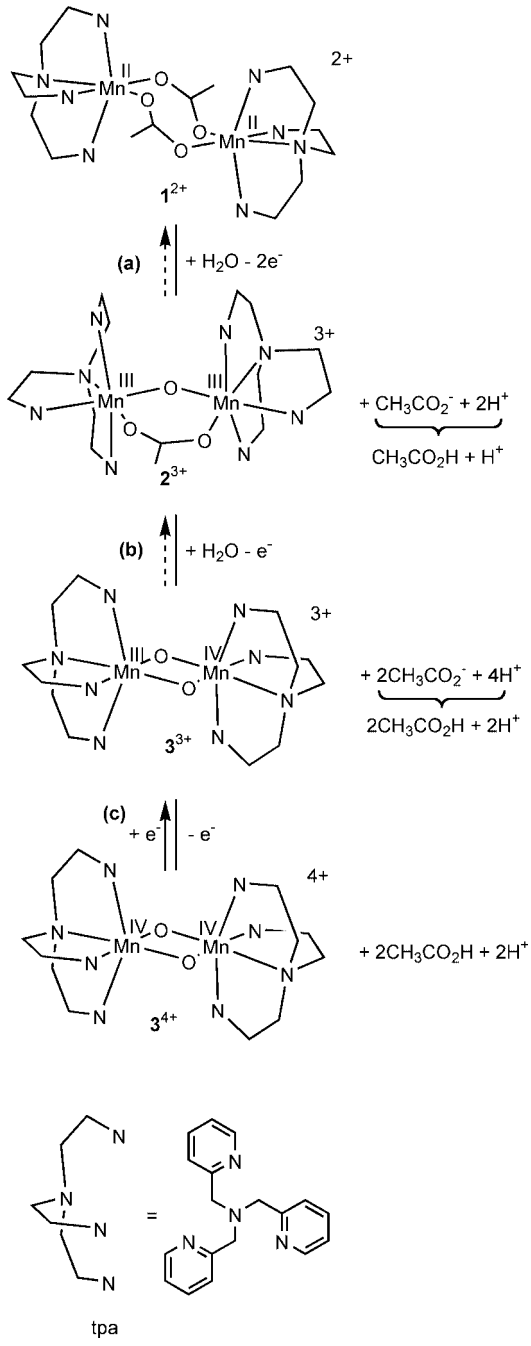

Scheme 1. Electrochemical interconversions of dinuclear manganese tpa complexes.

Electrochemistry

As we will see, the oxidation of $\mathbf{1}^{2+}$ in CH_3CN is a fully irreversible process that leads first to the mono-(μ-oxo)/mono-(μ-acetato) complex $\mathbf{2}^{3+}$ and then the bis(μ-oxo) complex $\mathbf{3}^{4+}$ (Scheme 1). For a better understanding of the processes involved, the electrochemical behavior of $\mathbf{3}^{3+}$ is first presented, and then those of complexes $\mathbf{2}^{3+}$ and $\mathbf{1}^{2+}$. All the potentials are referenced to an Ag/0.01 M $AgNO_3$ reference electrode in CH_3CN + 0.1 M Bu_4NClO_4. Potentials referred to this system can be converted to the ferrocene/ferrocenium couple by subtracting 87 mV, or to SCE or NHE by adding 298 or 548 mV, respectively.[42]

Electrochemical Behavior of $[Mn_2^{III,IV}(O)_2(tpa)_2](ClO_4)_3$ [$3(ClO_4)_3$]

As previously observed by Suzuki et al.,[38] the cyclic voltammogram of a CH_3CN solution of $\mathbf{3}^{3+}$ in the presence of 0.1 M Bu_4NClO_4 (Figure 2, A) displays a single reversible oxidation wave at $E^{3A}_{1/2}$ = 0.77 V (E^{3A}_{pa} = 0.80 and E^{3A}_{pc} = 0.74 V; ΔE_p = 60 mV) and one reversible reduction wave at $E^{3B}_{1/2}$ = –0.05 V (E^{3B}_{pc} = –0.08 and E^{3B}_{pa} = –0.02 V; ΔE_p = 60 mV) corresponding to Equations (1) and (2), respectively.

$$[Mn_2^{III,IV}(O)_2(tpa)_2]^{3+} \rightleftharpoons [Mn_2^{IV,IV}(O)_2(tpa)_2]^{4+} + e^- \quad (1)$$
$$\mathbf{3}^{3+} \qquad\qquad \mathbf{3}^{4+}$$

$$[Mn_2^{III,IV}(O)_2(tpa)_2]^{3+} + e^- \rightleftharpoons [Mn_2^{III,III}(O)_2(tpa)_2]^{2+} \quad (2)$$
$$\mathbf{3}^{3+} \qquad\qquad \mathbf{3}^{2+}$$

Exhaustive electrolyses of solutions of this complex confirm the excellent stability of the $Mn_2^{III,III}$ ($\mathbf{3}^{2+}$) and $Mn_2^{IV,IV}$ ($\mathbf{3}^{4+}$) species. Exhaustive reduction of a solution of $\mathbf{3}^{3+}$ at –0.2 V consumes one electron per molecule of complex and leads to the quasi-quantitative formation of the one-electron-reduced species $\mathbf{3}^{2+}$ (yield: 97%). The yield is calculated from the relative height of the two waves [Equation (2)] of the voltammograms at a rotating disc electrode before and after reduction (Figure 2, B).

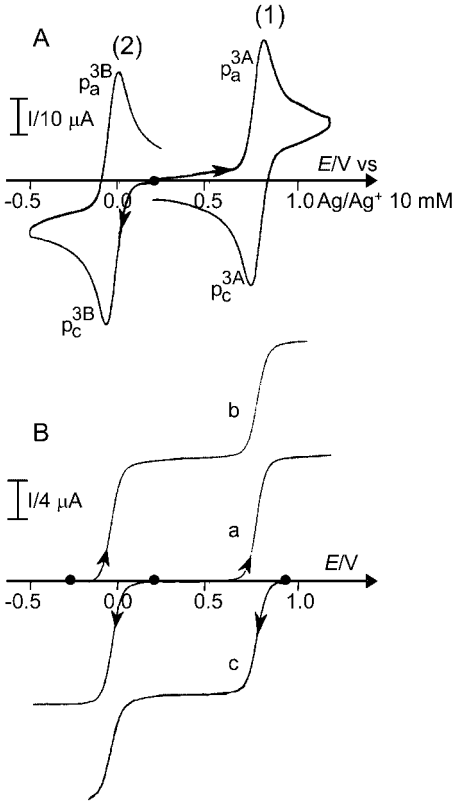

Figure 2. (A) Cyclic voltammograms at a Pt electrode (diameter: 5 mm) of a 0.72 mM solution of $\mathbf{3}^{3+}$ in CH_3CN + 0.1 M Bu_4NClO_4; sweep rate: 100 mV s^{-1}; (B) voltamperograms at a Pt rotating disc electrode (diameter: 0.2 mm); rotation speed: 600 min^{-1}; sweep rate: 10 mV s^{-1}: (a) solution (A), (b) solution (A) after exhaustive reduction at –0.2 V (formation of $\mathbf{3}^{2+}$), and (c) after exhaustive oxidation of a solution of a 0.72 mM of $\mathbf{3}^{3+}$ in CH_3CN + 0.1 M Bu_4NBF_4 at 0.9 V (formation of $\mathbf{3}^{4+}$). The numbers in parentheses correspond to the equation number in the text.

On the other hand, as previously reported,[38] exhaustive oxidation of a solution of $\mathbf{3}^{3+}$ at 0.9 V in CH_3CN in the presence of 0.1 M Bu_4NClO_4 leads to the formation of a green precipitate corresponding to $\mathbf{3}^{4+}$. However, we were able to prevent the precipitation of $\mathbf{3}^{4+}$ by using Bu_4NBF_4 as supporting electrolyte instead of Bu_4NClO_4. This complex is formed in solution with a 95% yield after one electron has been consumed per molecule (Figure 2B). Figure 3 displays the absorption spectra of the different species in the visible region. The green (III,IV) complex $\mathbf{3}^{3+}$ (spectrum a) shows three bands in the visible region at 444 (ε = 1490 M^{-1} cm^{-1}), 560 (760), and 658 nm (620) and one band in the UV region at 258 nm (36850). The green (IV,IV) complex $\mathbf{3}^{4+}$ (spectrum c) exhibits three visible bands at 418, 534 and 642 nm. This spectrum is similar to that obtained by Suzuki et al.[38] after redissolution of the green precipitate of $[Mn_2^{IV,IV}(O)_2(tpa)_2](ClO_4)_4$ in CH_3CN in the absence of supporting electrolyte [418 (6000), 534 (1032), and 642 nm (1084)]. The pale-yellow (III,III) complex (spectrum b) does not exhibit any well-resolved bands in the visible region.[36]

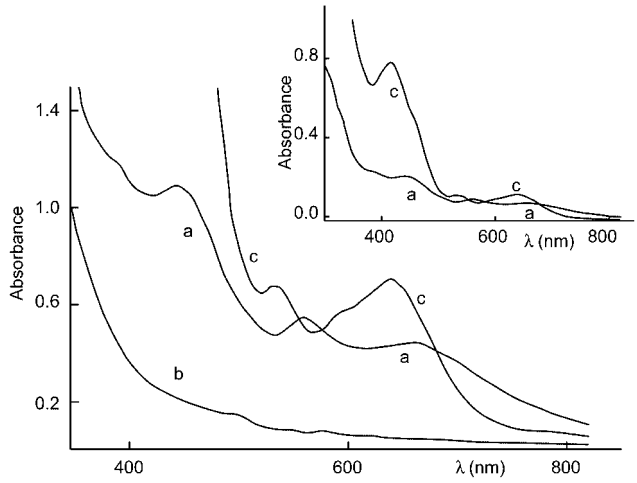

Figure 3. Visible absorption spectra of a 0.72 mM solution of $\mathbf{3}^{3+}$ in CH_3CN + 0.1 M Bu_4NClO_4: (a) initial solution, (b) solution (a) after exhaustive reduction at –0.2 V, and (c) after exhaustive oxidation of a 0.72 mM solution of $\mathbf{3}^{3+}$ in CH_3CN + 0.1 M Bu_4NBF_4 at 0.9 V; l = 1 cm; inset: l = 2 mm.

Electrochemical Behavior of $[Mn_2^{III}(O)(O_2CCH_3)(tpa)_2](PF_6)_3\cdot CH_3CN$ [2(PF$_6$)$_3$·CH$_3$CN]

Figure 4 shows the visible absorption spectrum of $\mathbf{2}^{3+}$. This pale purple/red complex exhibits two visible absorption bands at 494 (ε = 520 M^{-1} cm^{-1}) and 532 nm (440) corresponding to d-d transitions and a broad absorption band centerd at 720 nm (185). This spectrum is similar to those reported for other complexes possessing the same $\{Mn_2(O)(O_2CCH_3)\}^{3+}$ core.[39–41] The cyclic voltammogram of this complex in CH_3CN containing 0.1 M Bu_4NBF_4 (scan rate of 100 mV s^{-1}) displays three waves at $E_{1/2}^{2A}$ = 0.95 V (E_{pa}^{2A} = 1.00 and E_{pc}^{2A} = 0.90 V; ΔE_p = 100 mV),

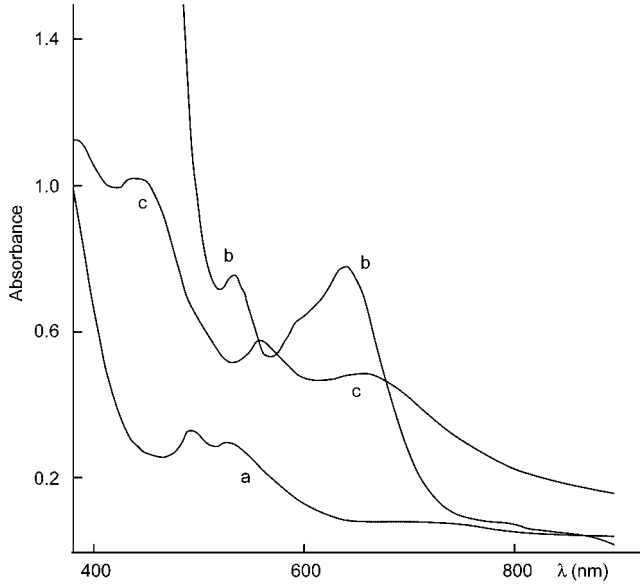

Figure 4. Visible absorption spectra of a 0.77 mM solution of $\mathbf{2}^{3+}$ in CH_3CN + 0.1 M Bu_4NBF_4: (a) initial solution, (b) solution (a) after exhaustive oxidation at 1.15 V, and (c) solution (b) after exhaustive reduction at 0.6 V; l = 1 cm.

$E_{1/2}^{2B}$ = 1.45 V (E_{pa}^{2B} = 1.49 and E_{pc}^{2B} = 1.41 V; ΔE_p = 80 mV); $E_{1/2}^{2C}$ = –0.07 V (E_{pc}^{2C} = –0.12 and E_{pa}^{2C} = –0.02 V; ΔE_p = 100 mV; Figure 5, A). The two oxidation waves are reversible and are attributed to the redox couples $Mn_2^{III,III/III,IV}$ and $Mn_2^{III,IV/IV,IV}$ [Equations (3) and (4), respectively].

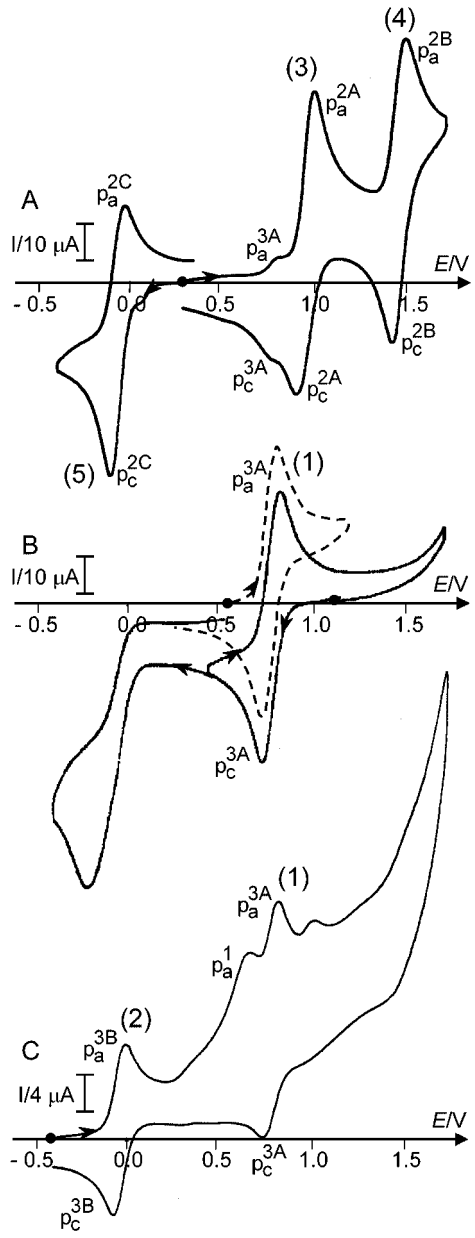

Figure 5. (A) Cyclic voltammograms at a Pt electrode (diameter: 5 mm) of a 0.77 mM solution of $\mathbf{2}^{3+}$ in CH_3CN + 0.1 M Bu_4NBF_4; scan rate: 100 mV s^{-1}; (B) solution (A) after exhaustive oxidation at 1.15 V [curve (–), formation of $\mathbf{3}^{4+}$], then exhaustive reduction at 0.6 V [curve (----), formation of $\mathbf{3}^{3+}$], and (C) after exhaustive reduction of a 0.3 mM solution of $\mathbf{2}^{3+}$ at –0.4 V (formation of $\mathbf{1}^{2+}$ and $\mathbf{3}^{2+}$); scan rate: 100 mV s^{-1}. The numbers in parentheses correspond to the equation number in the text.

The reduction wave, which is only partially reversible at that scan rate, is associated with the redox states $Mn_2^{III,III/III,II}$ [Equation (5)].

$$[Mn_2^{III}(O)(O_2CCH_3)(tpa)_2]^{3+} \rightleftharpoons [Mn_2^{III,IV}(O)(O_2CCH_3)(tpa)_2]^{4+} + e^- \quad (3)$$
$$\mathbf{2}^{3+} \qquad\qquad \mathbf{2}^{4+}$$

$$[Mn_2^{III,IV}(O)(O_2CCH_3)(tpa)_2]^{4+} \rightleftharpoons [Mn_2^{IV}(O)(O_2CCH_3)(tpa)_2]^{5+} + e^- \quad (4)$$
$$\mathbf{2}^{4+} \qquad\qquad \mathbf{2}^{5+}$$

$$[Mn_2^{III}(O)(O_2CCH_3)(tpa)_2]^{3+} + e^- \rightleftharpoons [Mn_2^{III,II}(O)(O_2CCH_3)(tpa)_2]^{2+} \quad (5)$$
$$\mathbf{2}^{3+} \qquad\qquad \mathbf{2}^{2+}$$

The additional reversible wave with low intensity located at $E_{1/2}^{3A}$ = 0.77 V corresponds to an impurity of about 8% of the bis(μ-oxo) complex $\mathbf{3}^{3+}$ present in the sample (see below). None of the oxidized or reduced species of $\mathbf{2}^{3+}$ are stable over the timescale of a controlled potential electrolysis.

Exhaustive oxidation of a solution of $\mathbf{2}^{3+}$ at a potential of 1.15 V consumes about two electrons per molecule of complex and leads to the quasi-quantitative formation of the di-μ-oxo $Mn_2^{IV,IV}$ complex $\mathbf{3}^{4+}$. The formation of this complex is the result of the instability of the one-electron-oxidized form of $\mathbf{2}^{3+}$ $[Mn_2^{III,IV}(O)(O_2CCH_3)(tpa)_2]^{4+}$ [Equation (3)], which reacts with residual water in the solvent[25–29,43] to form the binuclear complex $\mathbf{3}^{3+}$ by substitution of one acetato bridge by an oxo bridge [Equation (6)].

$$[Mn_2^{III,IV}(O)(O_2CCH_3)(tpa)_2]^{4+} + H_2O \rightleftharpoons [Mn_2^{III,IV}(O)_2(tpa)_2]^{3+} + CH_3CO_2^- + 2\,H^+ \quad (6)$$
$$\mathbf{2}^{4+} \qquad\qquad \mathbf{3}^{3+}$$

However, since $\mathbf{3}^{3+}$ is more easily oxidizable than $\mathbf{2}^{3+}$ ($E_{1/2}^{3A}$ = 0.77 and $E_{1/2}^{2A}$ = 0.95 V, respectively), $\mathbf{3}^{3+}$ is oxidized to $\mathbf{3}^{4+}$ at the electrolysis potential used for the oxidation of $\mathbf{2}^{2+}$ [E = 1.15 V; Equation (1)]. Equation (7) summarises the overall reaction.

$$[Mn_2^{III}(O)(O_2CCH_3)(tpa)_2]^{3+} + H_2O \rightleftharpoons [Mn_2^{IV}(O)_2(tpa)_2]^{4+} + CH_3CO_2^- + 2\,H^+ + 2e^- \quad (7)$$
$$\mathbf{2}^{3+} \qquad\qquad \mathbf{3}^{4+}$$

It should be noted that if one of the two protons released is trapped by the acetate anion released, the other one does not interact with $\mathbf{3}^{4+}$ since the formation of this complex is quasi-quantitative, as estimated by electrochemistry and by visible absorption spectroscopy (Figure 4, spectrum b). The cyclic voltammogram obtained after oxidation (Figure 5, B) shows the one-electron reversible wave at $E_{1/2}^{3A}$ = 0.77 V which is typical of the electroactivity of $\mathbf{3}^{4+}$, $[Mn_2^{IV,IV}/$

$Mn_2^{III,IV}$ couple; Equation (1)] and is followed by a second irreversible system at –0.21 V corresponding to the reduction of $\mathbf{3}^{3+}$. The irreversibility of this latter system is due to the presence of both acetate anions and protons released during the oxidation in solution [Equation (7)].

Indeed, under these particular conditions the reduction of the electrolyzed solution of $\mathbf{3}^{4+}$ at –0.4 V (three electrons consumed per initial molecule of $\mathbf{2}^{3+}$) does not lead selectively to the complex $\mathbf{3}^{2+}$ but to an equimolar mixture of complexes $\mathbf{3}^{2+}$ and $\mathbf{1}^{2+}$, as for the direct reduction of the initial solution of $\mathbf{2}^{3+}$ at this potential (see below). If the electrolyzed solution of $\mathbf{3}^{4+}$ is reduced at 0.6 V (consumption of about one electron per molecule of initial complex $\mathbf{2}^{3+}$), $\mathbf{3}^{3+}$ is obtained [Equation (1), Figure 5, B (dashed curve].

Exhaustive reduction of a solution of complex $\mathbf{2}^{3+}$ at a controlled potential of –0.4 V consumes one electron per molecule of complex. The resulting cyclic voltammogram (Figure 5, C) corresponds to the superimposition of the activity of complexes $\mathbf{3}^{2+}$ and $\mathbf{1}^{2+}$ (see below). The respective amount of both complexes was estimated from the height of the different waves at the rotating disc electrode and corresponds, for each complex, to half of the initial concentration of $\mathbf{2}^{3+}$. The reduction mechanism of $\mathbf{2}^{3+}$ involves the initial formation of the unstable species $\mathbf{2}^{2+}$ [Equation (5)] which undergoes a disproportionation reaction to give the stable final species $\mathbf{1}^{2+}$ and $\mathbf{3}^{2+}$ [Equation (8)].

$$[Mn_2^{II,III}(O)(O_2CCH_3)(tpa)_2]^{2+} \rightleftharpoons \underset{\mathbf{2}^{2+}}{} \quad (8)$$

$$\tfrac{1}{2}\,[Mn_2^{II}(O_2CCH_3)_2(tpa)_2]^{2+} + \tfrac{1}{2}\,[Mn_2^{III}(O)_2(tpa)_2]^{2+}$$
$$\mathbf{1}^{2+} \qquad\qquad \mathbf{3}^{2+}$$

Equation (9) summarises the overall process.

$$[Mn_2^{III}(O)(O_2CCH_3)(tpa)_2]^{3+} + e^- \rightleftharpoons \underset{\mathbf{2}^{3+}}{} \quad (9)$$

$$\tfrac{1}{2}\,[Mn_2^{II}(O_2CCH_3)_2(tpa)_2]^{2+} + \tfrac{1}{2}\,[Mn_2^{III}(O)_2(tpa)_2]^{2+}$$
$$\mathbf{1}^{2+} \qquad\qquad \mathbf{3}^{2+}$$

The two oxidation waves of $\mathbf{2}^{3+}$ [Equations (3) and (4)] appear to be more reversible than those of $[Mn_2^{III}(O)(O_2CCH_3)_2(bpea)_2]^{2+}$ at the same scan rate.[29] This shows that the rate of formation of the bis(μ-oxo) complex $\mathbf{3}^{3+}$ is slower than that of $[Mn_2^{III,IV}(O)_2(O_2CCH_3)(bpea)_2]^{2+}$ due to the greater stability of $[Mn_2^{III,IV}(O)(O_2CCH_3)(tpa)_2]^{4+}$ compared to $[Mn_2^{III,IV}(O)(O_2CCH_3)_2(bpea)_2]^{3+}$.

Electrochemical Behavior of $[Mn_2^{II}(O_2CCH_3)_2(tpa)_2](PF_6)_2$ [1(PF$_6$)$_2$]

The cyclic voltammogram of a solution of $\mathbf{1}^{2+}$ in CH_3CN containing 0.1 M Bu_4NBF_4 displays a first irreversible oxidation peak at E_{pa}^{1} = 0.70 V corresponding to the oxidation of the metallic centers of the complex (Figure 6, A). This oxidation leads to the formation of $\mathbf{2}^{3+}$, as evidenced by the presence of its two partially reversible oxidation waves at $E_{1/2}^{2A}$ = 0.95 and $E_{1/2}^{2B}$ = 1.45 V, which follow the irreversible oxidation peak at 0.70 V, and by the irreversible reduction peak at –0.04 V in the reverse scan. Complex $\mathbf{3}^{3+}$, which is formed during the oxidation of $\mathbf{2}^{3+}$ at E_{pa}^{2A} = 1.0 V, is also detected in the cyclic voltammogram by the presence of its first reduction peak at E_{pc}^{3A} = 0.73 V. This electro-induced transformation is faster than the oxidation of $\mathbf{2}^{3+}$ into $\mathbf{3}^{3+}$ since the oxidation peak of $\mathbf{1}^{2+}$ is fully irreversible even for higher scan rates of up to 500 mV s^{-1}.

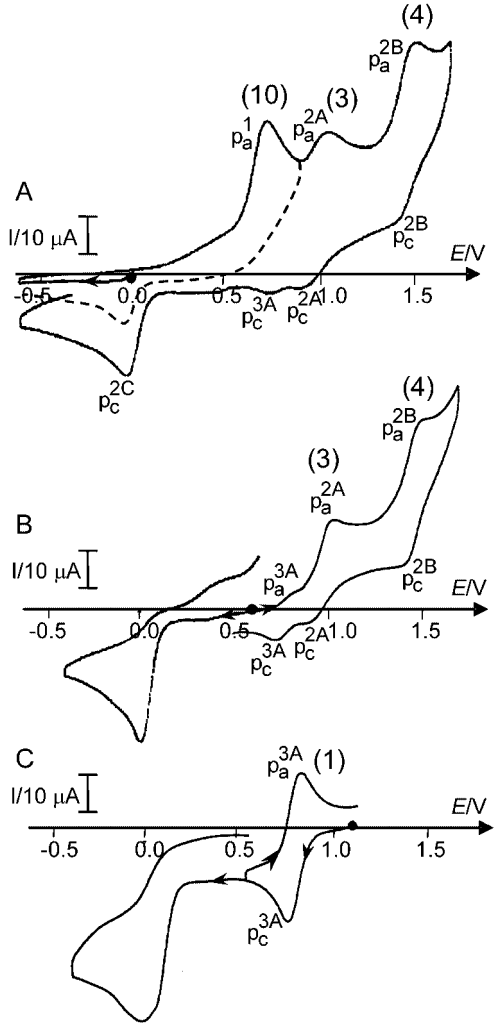

Figure 6. Cyclic voltammograms at a Pt electrode (diameter: 5 mm) of (A) a 0.45 mM solution of $\mathbf{1}^{2+}$ in CH_3CN + 0.1 M of Bu_4NClO_4; (B) solution (A) after exhaustive oxidation at 0.7 V (formation of $\mathbf{2}^{3+}$), and (C) solution (B) after exhaustive oxidation at 1.10 V (formation of $\mathbf{3}^{4+}$); scan rate: 100 mV s^{-1}. The numbers in parentheses correspond to the equation number in the text.

As expected, exhaustive oxidation of a solution of $\mathbf{1}^{2+}$ at 0.7 V consumes two electrons per molecule of complex and leads mainly to the formation of $\mathbf{2}^{3+}$ (yield: 90%). The resulting cyclic voltammogram displays the typical activity of this complex (Figure 6, B). However, a small amount of $\mathbf{3}^{3+}$ is also formed during the oxidation process (about 8%), as

attested by the presence of its reversible oxidation wave at $E^{3A}_{1/2}$ = 0.77 V. This explains why the same amount of this complex is present in the sample of $\mathbf{2}^{3+}$ isolated from electrolyzed solutions.

The processes involved in the oxidation of $\mathbf{1}^{2+}$ are summarized in Equation (10) [Scheme 1(a)].

$$\underset{\mathbf{1}^{2+}}{[Mn_2^{II}(O_2CCH_3)_2(tpa)_2]^{2+}} + H_2O \rightleftharpoons \underset{\mathbf{2}^{3+}}{[Mn_2^{III}(O)(O_2CCH_3)(tpa)_2]^{3+}} + CH_3CO_2^- + 2\,H^+ + 2\,e^- \quad (10)$$

As for the oxidation of $\mathbf{2}^{3+}$ into $\mathbf{3}^{4+}$ [Equation (7)], the oxidation of $\mathbf{1}^{2+}$ into $\mathbf{2}^{3+}$ leads to the dissociation of one acetate anion and the formation of an oxo bridge between the two manganese ions by deprotonation of a water molecule from the solvent.

Subsequent electrolysis at 1.10 V results in the quantitative formation of $\mathbf{3}^{4+}$ after the exchange of two additional electrons per molecule of the initial complex $\mathbf{1}^{2+}$ [Equation (7)] [Scheme 1 (b)]. The cyclic voltammogram of the resulting green solution (Figure 6, C), as well as the visible absorption spectrum, are typical of a solution of $\mathbf{3}^{4+}$. It should be noted that $\mathbf{3}^{4+}$ can be generated directly, with the same yield, by a four-electron oxidation of $\mathbf{1}^{2+}$ at 1.10 V [Equation (11); Scheme 1 (a–c)].

$$\underset{\mathbf{1}^{2+}}{[Mn_2^{II}(O_2CCH_3)_2(tpa)_2]^{2+}} + 2\,H_2O \rightleftharpoons \underset{\mathbf{3}^{4+}}{[Mn_2^{IV}(O)_2(tpa)_2]^{4+}} + 2\,CH_3CO_2^- + 4\,H^+ + 4\,e^- \quad (11)$$

The reaction in Equation (10) is an overall reversible process, therefore a controlled-potential reduction of the electrochemically generated solution of $\mathbf{2}^{3+}$ at –0.6 V completely restores the initial amount of $\mathbf{1}^{2+}$ [Scheme 1 (a)] after the consumption of two electrons per molecule of initial $\mathbf{1}^{2+}$. Likewise, the initial amount of $\mathbf{1}^{2+}$ can also be obtained by a controlled-potential reduction of the electrochemically generated solution of $\mathbf{3}^{4+}$ at –0.6 V [Equation (11); Scheme 1 (a–c)] after consumption of 3.8 electrons per molecule of $\mathbf{1}^{2+}$.

Discussion and Conclusion

We have systematically investigated the redox properties of three different cores $\{Mn_2^{II}(\mu\text{-}O_2CCH_3)_2\}$, $\{Mn_2^{III}(\mu\text{-}O)(\mu\text{-}O_2CCH_3)\}$, and $\{Mn_2^{III}(\mu\text{-}O)_2\}/\{Mn_2^{III,IV}(\mu\text{-}O)_2\}/\{Mn_2^{IV,IV}(\mu\text{-}O)_2\}$ with the same terminal ligand (tpa) and studied possible core interconversions between the various oxidation levels of manganese. Oxidation of the $\{Mn_2^{II}(\mu\text{-}O_2CCH_3)_2\}$ complex $\mathbf{1}^{2+}$ is fully irreversible and mainly leads to $\{Mn_2^{III}(\mu\text{-}O)(\mu\text{-}O_2CCH_3)\}$ ($\mathbf{2}^{3+}$). Further oxidation of $\mathbf{2}^{3+}$ yields the $\{Mn_2^{IV,IV}(\mu\text{-}O)_2\}$ complex $\mathbf{3}^{4+}$ quantitatively (Scheme 1). The rate of the electroinduced transformation of $\mathbf{1}^{2+}$ into $\mathbf{2}^{3+}$ is faster than that of $\mathbf{2}^{3+}$ into $\mathbf{3}^{4+}$, as shown by the shape of the cyclic voltammograms of $\mathbf{1}^{2+}$ and $\mathbf{2}^{3+}$, which attests to the greater instability of a $(\mu\text{-}O_2CCH_3)_2$ species at the $Mn_2^{II,III}$ oxidation level than that of a $(\mu\text{-}O)(\mu\text{-}O_2CCH_3)$ at the $Mn_2^{III,IV}$ oxidation level. In addition, $\mathbf{2}^{3+}$ and $\mathbf{3}^{4+}$ can be selectively generated owing to a good separation of the two two-electron oxidation waves [the oxidation potentials of $\mathbf{1}^{2+}$ and $\mathbf{2}^{3+}$ are 0.70 and 0.95 V vs. Ag/Ag^+ (10 mM), respectively]. The oxidation potential of $\mathbf{3}^{3+}$ (0.77 V) is located between the oxidation potentials of $\mathbf{1}^{2+}$ and $\mathbf{2}^{3+}$. These transformations ($\mathbf{1}^{2+}$ into $\mathbf{2}^{3+}$ and $\mathbf{2}^{3+}$ into $\mathbf{3}^{4+}$) are chemically reversible by reduction processes, although the two steps are not separated. Indeed, $\mathbf{1}^{2+}$ is directly and entirely regenerated by reduction of $\mathbf{3}^{4+}$ (or $\mathbf{3}^{3+}$). These core interconversions under oxidative and reductive conditions obviously occur concomitantly with protonation/deprotonation reactions at the bridging oxo groups.

We have also isolated and crystallographically characterized a new binuclear manganese complex in the tpa series ($\mathbf{2}^{3+}$), which shows that the (III,III) oxidation state in the tpa series is stable with two types of cores: a bis(μ-oxo) and a mono-(μ-oxo) mono-(μ-acetato). The difference in Mn···Mn separation across the four binuclear tpa compounds is 1.50 Å [$\{Mn_2^{II}(O_2CCH_3)_2\}$ 4.154(1), $\{Mn_2^{III}(O)(O_2CCH_3)\}$ 3.253, $\{Mn_2^{III}(O)_2\}$ 2.656(2), $\{Mn_2^{III,IV}(O)_2\}$ 2.643(1) Å].

These electrochemical and crystallographic results are in agreement with the hypothesis of the presence of one oxo bridge for the active site of MnCat in the $Mn_2^{III,III}$ oxidation state.

We are currently evaluating the ability of these tpa complexes to disproportionate hydrogen peroxide in order to compare their efficiencies to those of the parent bpea complexes. Indeed, although the electrochemical behavior of the bpea and tpa complexes are quite similar, the oxidation potentials of the bpea complexes are clearly lower (about 160–190 mV) than those of the tpa complexes owing to the presence of an additional acetate bridge, which has a more pronounced electron-donor character than that of pyridine. In addition, the rate of formation of the $Mn_2^{III,IV}$ complex $\mathbf{3}^{3+}$ by oxidation of the $Mn_2^{III,III}$ complex $\mathbf{2}^{3+}$ is slower than that of the tpa derivative. A different catalytic efficiency may therefore be expected for these two kinds of complexes.

Experimental Section

Materials: Acetonitrile (Rathburn, HPLC grade) was used as received and stored under argon in a glovebox. Tetra-*n*-butylammonium perchlorate (Bu_4NClO_4), tetra-*n*-butylammonium tetrafluoroborate (Bu_4NBF_4), and tetra-*n*-butylammonium hexafluorophosphate (Bu_4NPF_6) were purchased from Fluka and used as received.

Tris(2-pyridylmethyl)amine (tpa) and the complex $\mathbf{3}(ClO_4)_3$ were synthesized according to previously described methods.[38]

$[Mn_2^{II}(O_2CCH_3)_2(tpa)_2](PF_6)_2$ [$\mathbf{1}(PF_6)_2$]: A solution of $MnSO_4{\cdot}H_2O$ (38.2 mg, 0.227 mmol) in water (5 mL) was added to

a solution of tpa (66 mg, 0.227 mmol) in methanol (5 mL). After 25 min of stirring, a solution of $NaCH_3CO_2$ (19 mg, 0.227 mmol) in water (1 mL) was added. The resulting colorless solution was stirred at room temperature for 15 min. After addition of solid KPF_6 (82.2 mg, 0.446 mmol) the solution was evaporated to dryness and the yellow-white residue redissolved in CH_3CN. The solution was filtered to remove insoluble white K_2SO_4 and the filtrate was then evaporated to dryness. The colorless residue obtained was then redissolved in dichloromethane and the resulting solution filtered to remove a white powder corresponding to excess KPF_6. The filtrate was then evaporated to dryness and a pale-yellow powder corresponding to **1**$(PF_6)_2$ was obtained. Yield: 150 mg (60%). These crystals analyzed satisfactorily as $[Mn_2^{II}(\mu\text{-}O_2CCH_3)_2(tpa)_2](PF_6)_2$. $C_{40}H_{42}F_{12}Mn_2N_8O_4P_2$ (1098.6): calcd. C 43.71, H 3.85, N 10.2; found C 43.66, H3.91, N 10.12. IR (KBr): $\tilde{\nu}$ = 3428 cm^{-1} (m), 1605 (s), 1580 (s), 1505 (w), 1484 (m), 1444 (s), 1353 (w), 1294 (m), 1269 (w), 1158 (m), 1122 (w), 1100 (m), 1053 (m), 1017 (m), 840 (vs), 764 (s), 639 (m), 557 (s), 500 (w), 415 (w).

$[Mn_2^{III}(O)(O_2CCH_3)(tpa)_2](PF_6)_3$ [2$(PF_6)_3$]: This complex was synthesized by an electrochemical procedure. Exhaustive oxidation of a 4.5 mM solution of **1**$(PF_6)_2$ in 12 mL of CH_3CN containing 0.1 M Bu_4NPF_6 as supporting electrolyte at 0.80 V on a platinum plate led to formation of a red-purple solution corresponding to the complex $\mathbf{2}^{3+}$. Red-purple crystals of **2**$(PF_6)_3{\cdot}CH_3CN$ suitable for X-ray diffraction were grown after one day by slow vapor diffusion of diethyl ether into this solution. These were filtered, washed with CH_2Cl_2, and dried under air. Yield: 53.9 mg (85%). These crystals analyzed satisfactorily as **2**$(PF_6)_3$. $C_{38}H_{39}Mn_2N_8O_3P_3F_{18}$ (1200): calcd. C 37.93, H3.24, N 9.51; found C 38.00, H 3.25, N 9.33. IR (KBr): $\tilde{\nu}$ = 3445 cm^{-1} (vs), 1609 (s), 1574 (w), 1531 (w), 1487 (w), 1445 (s), 1295 (m), 1163 (m), 1101 (m), 1063 (m), 1032 (m), 1023 (m), 839 (vs), 761 (m), 707 (m), 678 (m), 661 (m), 614 (m), 557 (s), 414 (w). UV/Vis (CH_3CN): λ_{max} (ε) = 256 nm (20640 $M^{-1}cm^{-1}$), 289 (10910, sh), 380 (1160, sh), 494 (410), 532 (350), 720 (150).

Spectroscopy: Infrared spectra were recorded with a Perkin–Elmer Spectrum GX FTIR spectrometer. Electronic absorption spectra were recorded with a Cary 50 Varian spectrophotometer. Initial and electrolyzed solutions were transferred into a conventional cuvette cell in a glovebox. The cell was inserted into an optical translator connected to the spectrophotometer through a fiber optic system (Photonetics Spectrofip System). The optical fibers pass through the wall of the dry box via seals.

Electrochemical Measurements: All electrochemical measurements were run under argon in a dry glovebox at room temperature. Cyclic voltammetry (CV) and controlled potential electrolysis experiments were performed using an EG&G PAR model 173 potentiostat equipped with a PAR model universal programmer and a PAR model 179 digital coulometer. The electrolyte was a 0.1 M solution of Bu_4NClO_4, Bu_4NBF_4, or Bu_4NPF_6 in CH_3CN. A standard three-electrode electrochemical cell was used. Potentials were referred to an Ag/10 mM $AgNO_3$ reference electrode in CH_3CN (+0.1 M Bu_4NClO_4). The working electrodes were 5-mm-diameter platinum disks polished with 2-μm diamond paste for cyclic voltammetry [E_{pa}: anodic peak potential; E_{pc}: cathodic peak potential; $E_{1/2} = (E_{pa} + E_{pc})/2$; $\Delta E_p = E_{pa} - E_{pc}$] and 2-mm-diameter disks for rotating disk electrode experiments (RDE). Exhaustive electrolyses were carried out with a 5 cm^2 platinum cylinder or a 10×10×4 mm^3 carbon felt electrode (RCV, 2000, 65 mg cm^{-3}, from Le Carbone Lorraine). The counter electrode was a Pt wire in CH_3CN (+0.1 M Bu_4NClO_4, Bu_4NBF_4, or Bu_4NPF_6).

Crystal-Structure Determination of 2$(PF_6)_3{\cdot}CH_3CN$: A crystal of **2**$(PF_6)_3{\cdot}CH_3CN$ of dimensions 0.5×0.4×0.08 mm^3 was selected. Diffraction data were collected with a Bruker SMART diffractometer with Mo-K_α radiation. All calculations were performed using the SHELXTL computer program.[44] The structure was solved by direct methods and refined by full-matrix least-squares fits on F^2. The crystallographic data are summarized in Tables 1 and 2.

Table 2. Principal crystallographic data and parameters for $[Mn_2^{III}(O)(O_2CCH_3)(tpa)_2](PF_6)_3{\cdot}CH_3CN$ [**2**$(PF_6)_3{\cdot}CH_3CN$].

Compound	$[Mn_2^{III}(O)(O_2CCH_3)(tpa)_2](PF_6)_3{\cdot}CH_3CN$
Chemical formula	$C_{40}H_{42}F_{18}Mn_2N_9O_3P_3$
Formula weight	1241.62
Crystal system	monoclinic
Space group	$P2_1/n$
a [Å]	11.9899(17)
b [Å]	35.050(5)
c [Å]	12.3952(18)
β [°]	101.218(6)
V [Å^3]	5109.5(13)
T [K]	223(2)
λ [Å]	0.71073
Density [mg m^{-3}]	1.614
Z	4
μ [mm^{-1}]	0.701
F(000)	2504
Reflections collected	10619
R_1[a]	0.0514
wR_2[b]	0.1048

[a] $R_1 = \Sigma||F_o| - |F_c||/\Sigma|F_o|$. [b] $wR = [\Sigma w(|F_o| - |F_c|)^2/\Sigma wF_o^2]^{1/2}$.

CCDC-625212 contains the supplementary crystallographic data for this paper. These data can be obtained free of charge from the Cambridge Crystallographic Data Center via www.ccdc.cam.ac.uk/datarequest/cif.

Acknowledgments

The authors acknowledge Dr. J.-M. Latour from the Laboratoire de Physicochimie des Métaux en Biologie, DRDC, UMR 5155 CEA-CNRS-UJF, CEA-Grenoble for a gift of **3**$(ClO_4)_3$. This research was supported by the COST D21 program.

[1] J. Wu, J. E. Penner-Hahn, V. L. Pecoraro, *Chem. Rev.* **2004**, *104*, 903 and references cited therein.
[2] S. Mukhopadhyay, S. K. Mandal, S. Bhaduri, W. H. Armstrong, *Chem. Rev.* **2004**, *104*, 3981 and references cited therein.
[3] D. C. Weatherburn, S. Mandal, S. Mukhopadhyay, S. Bahduri, L. F. Lindoy, Manganese, in *Comprehensive Coordination Chemistry II* (Eds.: J. A. McCleverty, T. J. Meyer), Elsevier Pergamon, Oxford, **2004**, vol. 5, p. 1.
[4] S. Antonyuk, V. Melik-Adamyan, A. Popov, V. Lamzin, P. Hempstead, P. Harrison, P. Artymyuk, V. Barynin, *Crystallogr.* **2000**, *45*, 105.
[5] M. M. Whittaker, V. V. Barynin, T. Igarashi, J. W. Whittaker, *Eur. J. Biochem.* **2003**, *270*, 1102.
[6] V. V. Barynin, P. D. Hempstead, A. A. Vagin, S. V. Antonyuk, W. R. Melik-Adamyan, V. S. Lamzin, P. M. Harrison, P. J. Artymiuk, *J. Inorg. Biochem.* **1997**, *67*, 196 and references cited therein.
[7] V. V. Barynin, M. M. Whittaker, S. V. Antonyuk, V. S. Lamzkin, P. M. Harrison, P. J. Artymiuk, J. W. Whittaker, *Structure* **2001**, *9*, 725 and references cited therein.
[8] T. L. Stemmer Jr, T. M. Sossong, J. I. Goldstein, D. E. Ash, T. E. Elgren Jr, D. M. Kurtz, J. E. Penner-Hahn, *Biochemistry* **1997**, *36*, 9847.
[9] B. Kok, B. Forbush, M. McGloin, *Photochem. Photobiol.* **1970**, *11*, 457.

[10] P. Joliot, G. Barbieri, R. Chabaud, *Photochem. Photobiol.* **1969**, *10*, 309.
[11] M. Haumann, P. Liebisch, C. Müller, M. Barra, M. Grabolle, H. Dau, *Science* **2005**, *310*, 1019.
[12] J. E. Penner-Hahn, C. Yocum, *Science* **2005**, *310*, 982.
[13] J. P. McEvoy, J. A. Gascon, V. S. Batista, G. W. Brudvig, *Photochem. Photobiol.* **2005**, *4*, 940.
[14] M. Haumann, C. Müller, P. Liebisch, L. Iuzzolino, J. Dittmer, M. Grabolle, T. Neisius, W. Meyer-Klaucke, D. Dau, *Biochemistry* **2005**, *44*, 1894 and references cited therein.
[15] J. P. McEvoy, G. W. Brudvig, *Chem. Rev.* **2006**, *106*, 4457.
[16] R. D. Britt, J. M. Peloquin, K. A. Campbell, *Annu. Rev. Biophys. Biomol. Struct.* **2000**, *29*, 463.
[17] P. Glatzel, U. Bergmann, J. Yano, H. Visser, J. H. Robblee, W. Gu, F. M. F. de Groot, G. Christou, V. L. Pecoraro, S. P. Cramer, V. K. Yachandra, *J. Am. Chem. Soc.* **2004**, *126*, 9946 and references cited therein.
[18] V. K. Yachandra, K. Sauer, M. P. Klein, *Chem. Rev.* **1996**, *96*, 2927.
[19] A. Zouni, H.-T. Witt, J. Kern, P. Fromme, N. Krauβ, W. Saenger, P. Orth, *Nature* **2001**, *409*, 739.
[20] N. Kamiya, J.-R. Shen, *Proc. Natl. Acad. Sci. USA* **2003**, *100*, 98.
[21] K. N. Ferreira, T. M. Iverson, K. Maghlaoui, J. Barber, S. Iwata, *Science* **2004**, *303*, 1831.
[22] J. Kern, B. Loll, A. Zouni, W. Saenger, K.-D. Irrgang, J. Biesiadka, *Photosynth. Res.* **2005**, *84*, 153.
[23] B. Loll, J. Kern, W. Saenger, A. Zouni, J. Biesiadka, *Nature* **2005**, *438*, 1040.
[24] T. Tanase, S. J. Lippard, *Inorg. Chem.* **1995**, *34*, 4682.
[25] S. Mahapatra, P. Das, R. Mukherjee, *J. Chem. Soc., Dalton Trans.* **1993**, 217.
[26] S. Mahapatra, T. K. Lal, R. Mukherjee, *Inorg. Chem.* **1994**, *33*, 1579.
[27] T. K. Lal, R. Mukherjee, *Inorg. Chem.* **1998**, *37*, 2373.
[28] M.-N. Collomb Dunand-Sauthier, A. Deronzier, I. Romero, *J. Electroanal. Chem.* **1997**, *436*, 219.
[29] I. Romero, L. Dubois, M.-N. Collomb, A. Deronzier, J.-M. Latour, J. Pécaut, *Inorg. Chem.* **2002**, *41*, 1795.
[30] A. E. M. Boelrijk, S. V. Khangulov, G. C. Dismukes, *Inorg. Chem.* **2000**, *39*, 3009.
[31] L. Dubois, R. Caspar, L. Jacquamet, P.-E. Petit, M.-F. Charlot, C. Baffert, M.-N. Collomb, A. Deronzier, J.-M. Latour, *Inorg. Chem.* **2003**, *42*, 4817.
[32] L. P. Nielsen, M. Mortensen, S. Kjaergaard Knudsen, K.-L. Lund, M.-N. Collomb, C. Baffert, A. Deronzier, J.-M. Latour, N. Thorup, C. J. KcKenzie, *Dalton Trans.* **2003**, 1765.
[33] C. Hureau, S. Blanchard, M. Nierlich, G. Blain, E. Rivière, J.-J. Girerd, E. Anxolabéhères-Mallart, G. Blondin, *Inorg. Chem.* **2004**, *43*, 4415.
[34] A. Magnuson, P. Liebisch, J. Högblom, M. F. Anderlund, R. Lomoth, W. Meyer-Klaucke, M. Haumann, H. Dau, *J. Inorg. Biochem.* **2006**, *100*, 1234.
[35] H. Oshio, E. Ino, I. Mogi, T. Ito, *Inorg. Chem.* **1993**, *32*, 5697.
[36] Y. Hitomi, A. Ando, H. Matsui, T. Ito, T. Tanaka, S. Ogo, T. Funabiki, *Inorg. Chem.* **2005**, *44*, 3473.
[37] D. K. Towle, C. A. Botsford, D. J. Hodgson, *Inorg. Chim. Acta* **1988**, *141*, 167.
[38] M. Suzuki, S. Tokura, M. Suhara, A. Uehara, *Chem. Lett.* **1988**, 1763.
[39] N. Arulsamy, J. Glerup, A. Hazell, D. J. Hodgson, C. J. McKenzie, H. Toftlund, *Inorg. Chem.* **1994**, *33*, 3023.
[40] K. J. Oberhausen, R. J. O'Brien, J. F. Richardson, R. M. Buchanan, R. Costa, J.-M. Latour, H.-L. Tsai, D. N. Hendrickson, *Inorg. Chem.* **1993**, *32*, 4561.
[41] M. U. Triller, W.-Y. Hsieh, V. L. Pecoraro, A. Rompel, B. Krebs, *Inorg. Chem.* **2002**, *41*, 5544.
[42] V. V. Pavlishchuk, A. W. Addison, *Inorg. Chim. Acta* **2000**, *298*, 97.
[43] M. M. Morrison, D. T. Sawyer, *Inorg. Chem.* **1978**, *17*, 333.
[44] G. M. Sheldrick, *SHELXTL-Plus*, vers. 5.1, Structure Determination Software Programs, Bruker-AXS Inc., Madison, WI, **1998**.

Received: November 20, 2006
Published Online: March 20, 2007

